Smart Materials and Structures

Piezoelectric shell FE for the static and dynamic analysis of piezoelectric fibre composite laminates

To cite this article: Ahmad E Guennam and Bibiana M Luccioni 2009 *Smart Mater. Struct.* **18** 095044

View the article online for updates and enhancements.

Related content

- FE modeling of a closed box beam with piezoelectric fiber composite patches
  A E Guennam and B M Luccioni
- A piezolaminated composite degenerated shell finite element for active control of structureswith distributed piezosensors and actuators
  V Balamurugan and S Narayanan
- Modeling and analysis of smart piezoelectric beams using simple higher order shear deformation theory
  M Adnan Elshafei and Fuzy Alraiess

Recent citations

- A layered shell containing patches of piezoelectric fibers and interdigitated electrodes: Finite element modeling and experimental validation
  Bo B Nielsen *et al*
- Model for Piezoelectric/Ferroelectric composites polarized with interdigitated electrodes
  Ahmad Eduardo Guennam and Bibiana M. Luccioni
- Exact analysis for static response of cross ply laminated smart shells
  A.A. Khdeir and O.J. Aldraihem

This content was downloaded from IP address 190.3.119.146 on 25/04/2019 at 20:37

Smart Mater. Struct. **18** (2009) 095044 (12pp) doi:10.1088/0964-1726/18/9/095044

Piezoelectric shell FE for the static and dynamic analysis of piezoelectric fibre composite laminates

Ahmad E Guennam and Bibiana M Luccioni

CONICET, Avenida Rivadavia 1917, Buenos Aires, Argentina
and
Structures Institute, National University of Tucumán, Avenida Roca 1800, SM de Tucumán, Argentina

E-mail: eguennam@herrera.unt.edu.ar

Received 9 April 2009, in final form 29 June 2009
Published 17 August 2009
Online at stacks.iop.org/SMS/18/095044

Abstract
A piezoelectric multilamina shell FE developed to model thin walled structures with piezoelectric fibre composites polarized with interdigitated electrodes (PFCPIE) is proposed in this paper. A new scheme for the interpolation of the electric field is presented. The electric field in each lamina lies parallel to the lamina plane and coincides with the poling direction. Each piezoelectric lamina admits an arbitrary poling direction. Based on Reissner–Mindlin assumptions and a multilaminate approach, the element employs a single layer assumption for the mechanical displacements and a layerwise constant electric potential. An MITC strategy is used to avoid shear locking.

Two static examples are presented. The first is a cantilever piezoactuated beam and the second a single cell closed box beam with piezoelectric actuators.

The results obtained for the cantilever beam with the present formulation are compared with those obtained with native ABAQUS plane stress elements and an analytical solution. For the closed box beam the numerical results were compared with experimental results from the literature. Very encouraging results are obtained in both cases.

Finally, for the piezoactuated closed box beam, the FE model is used to obtain a state space model (SS). Based on the SS model, the design of the control system and the assessment of the system performance are carried out. Important systems characteristics are captured by the model, i.e. attenuation levels, frequency response and control voltage levels. This reveals that the proposed FE can be used to model and assess structural behaviour in a relatively simple and efficient way.

(Some figures in this article are in colour only in the electronic version)

1. Introduction

Piezoelectric devices are successfully used in the feedback control of smart structures (Nam and Kim 1995) and this branch has grown noticeably in the last two decades. These advanced structures integrate the actions of distributed sensors, actuators and control electronics in such a way that they can respond adaptively to environmental changes in a predefined and useful manner (Balamurugan and Narayan 2008).

Two decades ago, Crawley and de Luis (1987) proposed the use of piezoelectric devices in intelligent structures and since then, many authors have analysed the behaviour of many types of structures using those materials, (Sungsoo and Librescu 1998, Wang *et al* 1999, Balamurugan and Narayan 2001, Kekana 2003, Guennam and Luccioni 2006). Some aerospace applications for active materials include: active control vibrations of structures subjected to aeroelastic excitations (Wang and Quek 2002, Suleman and Costa 2004), noise attenuation (Balachandran *et al* 1996, Lim *et al* 1999), active structural acoustic control of sound transmission through aircraft and helicopter fuselages, and structural health monitoring (Monkhouse *et al* 2000). For

 © 2009 IOP Publishing Ltd Printed in the UK

Table 1. Material properties.

Material properties	Standard MFC (Park and Kim 2005)	AFC (Bent and Hagood 1997, DuPlessis and Hagood 1996)	Glass/epoxy	Aluminium
E_1 (GPa)	31.2	30.3	14.8	71
E_2 (GPa)	17.05	15.9	13.6	71
G_{12} (GPa)	5.12	5.52	1.9	26.7
ν_{12}	0.303	0.31	0.19	0.33
d_{11} ($\times 10^{-12}$ mV^{-1})	386.6	381	—	—
d_{12} ($\times 10^{-12}$ mV^{-1})	−175.5	−160	—	—
Electrode spacing 'p' (mm)	0.53	1.2	—	—
Density (kg m^{-3})	5115.9	4500	1800	2713

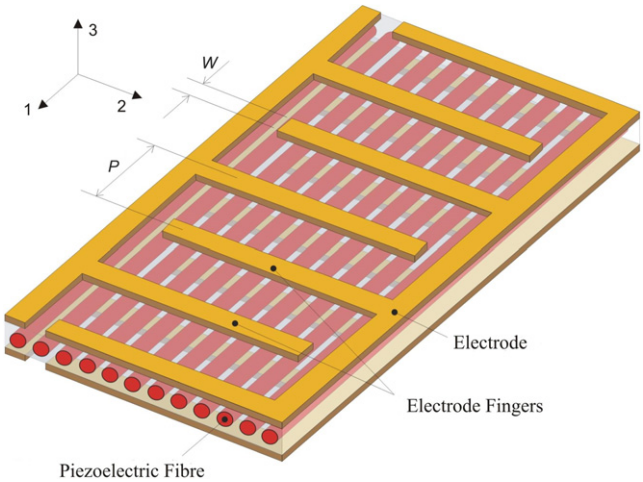

Figure 1. Piezoelectric fibre composite polarized with interdigitated electrodes (PFCPIE).

these applications piezoelectric materials are required to have an electromechanical coupling as high as possible with a minimum weight.

The anisotropic behaviour exhibited by piezoelectric materials makes the electromechanical coupling stronger in certain directions and very small, or practically nil, in others. This fact has encouraged the development of devices capable of introducing electric fields in those directions. With the development of piezoelectric fibres, actuators can be easily adapted to the host structure shape. Initially, metallic plates were used as electrodes generating an electric field orthogonal to the desired strain directions, '3-1 poling'. Later, with the introduction of interdigitated electrodes, the direction of the electric field could be matched with that of the desired strain, '1-1 poling', using piezoelectric fibres with the maximum coupling and improving the piezoelectric laminate performance (Bent and Hagood 1997).

Combining fibres and interdigitated electrodes, piezoelectric fibre composites polarized with interdigitated electrode (PFCPIE) patches and laminates, such as that schematically shown in figure 1, can be made.

The piezoelectric fibre composite may be of two types: the active fibre composite (AFC) or the macro-fibre composite (MFC). Both, AFC and MFC are anisotropic actuators with piezoelectric fibres embedded in a polymer matrix. AFC devices employ round cross-section PZT fibres, while rectangular cross-section piezoelectric fibres are used in MFC. In MFC the electrode fingers are closer to the fibres, which results in a more efficient transfer of the electric field into the fibres. This fact allows the use of lower electric potential levels with the same results. The paper by Park and Kim (2005) presents a detailed description of both composite types. Table 1 summarizes the electromechanical constitutive properties considered for AFC and MFC in the present work. Figure 1 corresponds to an AFC device.

From the analytical point of view, a computational tool that allows the designer to model the smart structure with its main features is of extreme interest. With these tools at hand, the performance of the smart structure under analysis could be evaluated for a different number of actuators and sensors (As/Ss) as well as for their disposition and size. The finite element method is a powerful tool in structural modelling. Finite elements capable of describing the structural behaviour of systems including piezoelectric materials can be considered as a generalization of those used in classical mechanical problems. The first finite element model that included the piezoelectric phenomenon was proposed by Allik and Hughes (1970). They presented a solid tetrahedral finite element. The first efforts were basically oriented to the study and design of piezoelectric transducers. Many related approaches have been developed lately (Varadan *et al* 1993).

As a result of the increasing interest in active structures, especially in the aerospace research field, other finite element formulations, more suitable for this type of application, have been developed. Because of the topology of the aeronautical structures, e.g. thin walled structures, efficient piezoelectric plate and shell elements are the main interest in this context. Here, efficiency is regarded as the ability of the element to represent the actual structure with a reasonable number of degrees of freedom. An efficient structural model is of great value because the nature of the problem is in essence a multiphysics one, i.e. the loads arise from the structure and the fluid interacting together while the controller injects the control signals, all in real time.

While searching for appropriate tools for the solution of this type of structural problem, involving piezoelectric materials, a great number of finite elements have been formulated. Benjeddou (2000) presents a survey on advances and tendencies in finite element modelling of smart structures that include piezoelectric materials.

Based on the classical and shear deformation shell and plate theories, finite elements that support piezoelectric

laminate composite materials are very popular in specialized literature (Reddy 1999). Two approaches can be distinguished for multilamina formulations (Kögl and Bucalem 2005a). In the first approach, in which displacement fields are assumed to be smooth across the thickness, the models are designated as equivalent single layer models. For the second approach, where the displacements are assumed to be smooth in each layer but not at the layers interfaces, the corresponding models are denoted as layerwise or zig-zag models (Carrera 1997, Saravanos *et al* 1997, Carrera 2002, 2003). These theories yield more accurate results, especially for thick laminates, and are better suited to predict interlaminar effects, but they lead to an increased overall number of degrees of freedom for the finite element model as compared to the equivalent single layer theories (Kögl and Bucalem 2005a).

As claimed by Kögl and Bucalem (2005b), the use of the Reissner–Mindlin assumptions, in the case of plates and shells, makes the elements suitable for both thin and moderately thick situations. A great number of finite element shells based on this assumption can be found.

Lammering (1991) developed a four-node shear deformable shell finite model, with a linear interpolation of displacements, rotations and electric potential inside the element. The finite element presents 7 degrees of freedom per node, three displacements, two rotations and two electric potentials, one for the upper face and another for the lower face. The model supports a three-layer laminate and generates an equivalent layer.

Suleman and Venkayya (1995) proposed a plate element based on Mindlin theory, with one electric potential degree of freedom for each layer, and used reduced numerical integration.

Thirupathi *et al* (1997) proposed an eight-noded isoparametric Reissner–Mindlin general shell element without nodal electric degree of freedom. The element is developed using a modified three-dimensional theory of shells. The piezoelectric effect is considered as an initial strain.

Saravanos *et al* (1997) assumed layerwise variation of the mechanical displacement and electrical potential fields. The resulting theory represents the kinematics of transverse section warping with more generality, and captures the nonlinear variation of the electric potential through the thickness for thick laminates.

Lee and Saravanos (2000) developed an eight-noded finite element shell based in a multilamina theory and linear thermopiezoelectricity. The proposed shell theory combines linear displacement fields through the thickness with layerwise electric potential and temperature fields through the laminate, consisting of N discrete continuous segments.

Chee *et al* (2000) proposed a model for multilayer configurations, with a cubic approximation of in-plane displacements, a quadratic approximation of out-of-plane displacement and a linear approximation of intralaminar potentials. Each layer can have an arbitrary orientation and can be piezoelectric or not. In addition to mechanical degrees of freedom, the values of the electric potential in each interlaminar interface and those correspondent to the external surfaces are included in the formulation. The approximation of the electric field is made in two steps. In the first step, the potential distribution functions in each interface are obtained using four nodes and standard isoparametric linear shape functions. In the second step, the electric field through the thickness is calculated assuming a linear intralaminar electric potential distribution.

Lammering and Mesecke-Rischmann (2003) analysed shell-like structures that have a core of conventional materials sandwiched between two piezoelectric patches. The authors presented different variational formulations and their correspondent finite element solutions, oriented to the design of different types of shell structures with piezoelectric patches. They formulated thick shell isoparametric elements based on Mindlin/Reissner theory. The structure kinematics is defined by the displacements corresponding to the passive zone and the piezoelectric layers. In this formulation a quadratic variation of the potential through the thickness, combined with a linear variation in the layer in terms of the nodal potentials, is assumed.

Similar approaches were used by Kögl and Bucalem (2005b) who formulated a family of piezoelectric MITC plate and shell elements and employed it for the modelling of multilayer smart structures.

Balamurugan and Narayan (2001) presented a formulation of a nine-noded piezolaminated degenerated shell finite element with a quadratic variation of the electric potential through the thickness.

As mentioned above, the amount of research work and the proposed tools for analysis and design of piezoelectric smart structures is very broad, especially when through the thickness polling devices are studied. However, the same does not apply for devices with tangential polling, specially polarized with interdigitated electrodes.

Guennam and Luccioni (2006) addressed finite element modelling of a closed box beam dotted with piezoelectric fibre composite patches. The finite element model was performed in ABAQUS (2006), employing piezoelectric solid brick C3D8E finite elements for the active zone and conventional shells S4 for the passive zone. Degrees of freedom constraints were introduced between nodes belonging to the same patch in order to control the electric field inside them via one single electric node per patch. A model order reduction was performed, and the stiffness and mass matrices were exported to MATLAB, where the control system was designed and assessed. The analysis clearly reveals the effect of the control system and the level of damping introduced. The use of brick elements for the patches results in a considerable number of degrees of freedom and additional complexity in introducing electric fields at the desired directions, especially when elements are not of a regular orthogonal shape. The aim of this paper is to present a piezoelectric shell finite element with a novel treatment for the electric field interpolation that allows the modelling of piezoelectric fibre composite laminates polarized with interdigitated electrodes in an easy and natural way with less degrees of freedom than those needed when solid elements are used.

The element is adequate for laminates considered to be made of one or more layers and each layer of different

material. Any combination of material types for the layers are allowed, i.e. monolithic, composite, piezoelectric, etc. This multilaminate model is based on a single layer assumption for the kinematic variables and a layerwise assumption for the electric potentials and electric field. With this tool at hand, it is possible to model smart thin walled structures, whose walls are made with many layers, some or all of which could be piezoelectric laminates polarized with an interdigitated electrode pattern (IEP). Independent control/sensing could be performed in each piezoelectric layer.

2. Shell finite element proposed

The smart structure could be obtained by bonding piezoelectric patches to a passive host structure as well as piezoelectric laminates embedded between passive laminae.

The use of piezoactuators and sensors of the '1-3' or '1-2' type demands the formulations of an FE with polarization and electric field vectors through the thickness. However, piezoelectric laminates polarized with interdigitated electrodes are of type '1-1' i.e. the poling and actuation direction are coincident. One of the objectives of this work is to represent this aspect in a direct manner in order to obtain reliable results.

Since in a general piezoelectric laminate each active layer may act as an actuator or sensor and constraints on the associated degrees of freedom are not *a priori* known, the layerwise theory for electric fields must be used.

For thick laminates, complete layerwise theories lead to more accurate results and are best suited for interlaminar effects predictions. However, the numerical cost is notably increased with respect to the single layer theory. For thin and moderately thick laminates, as far as the plane section assumption remains applicable, the single layer theory for kinematics variables combined with a layerwise theory for the electric fields seems to be a suitable balance between prediction accuracy and computational cost.

The IEP introduces a highly non-uniform electric field, whose magnitude and direction change between electrode fingers. In this case, it is very attractive to employ a homogenization technique to obtain the equivalent material properties (EMP), and a uniform electric field (UEF) running in the local parallel to the lamina direction. The EMP, combined with the UEF, behaves macroscopically like the actual device (Bent and Hagood 1997). The homogenization technique proposed by Bent and Hagood (1997) is used to obtain the electromechanical properties of the piezoelectric composite. After the homogenization, the resulting constitutive properties for each piezoelectric layer are obtained and the UEF is defined as $E = -\frac{\varphi}{p}$, where φ is the applied electric potential and p is the electrode spacing.

The physics involved in piezoelectric theory may be regarded as a coupling between Newton's second law and Maxwell's equations of electromagnetism (Joshi 1992). In the quasi-electrostatic approximation, the only electromagnetic equation which needs to be considered is the electric charge conservation equation. Then, the equations of the problem are the following,

$$\sigma_{ij,i} + \rho b_j = \rho \ddot{u}_j \tag{1}$$

$$D_{i,i} = q \tag{2}$$

where σ_{ij} is the Cauchy stress tensor, b_j is the body force vector, u_j is the displacement vector, ρ is the mass density, D_i is the electric displacement vector and q is the density of free electric charge.

The linear constitutive equations for a linear elastic piezoelectric media can be written as:

$$\sigma_{ij} = C_{ijkl}\varepsilon_{kl} - e_{kij}E_k \tag{3}$$

$$D_i = e_{ikl}\varepsilon_{kl} + \chi_{ik}E_k \tag{4}$$

where C_{ijkl} is the elastic stiffness tensor, e_{ikl} is the piezoelectric tensor and χ_{ik} is the electric permittivity tensor.

There are several possible approaches on which a piezoelectric finite element formulation can be based (Kögl and Bucalem 2005a, 2005b). Once the problem is stated in a weak form and a finite element method is employed to solve it, the following system of equations is obtained,

$$\begin{bmatrix} M_{\mathrm{mm}} & 0 \\ 0 & 0 \end{bmatrix} \begin{Bmatrix} \ddot{q}_{\mathrm{m}} \\ 0 \end{Bmatrix} + \begin{bmatrix} C_{\mathrm{mm}} & 0 \\ 0 & 0 \end{bmatrix} \begin{Bmatrix} \dot{q}_{\mathrm{m}} \\ 0 \end{Bmatrix} + \begin{bmatrix} K_{\mathrm{mm}} & K_{\mathrm{me}} \\ K_{\mathrm{em}} & K_{\mathrm{ee}} \end{bmatrix} \begin{Bmatrix} q_{\mathrm{m}} \\ q_{\mathrm{e}} \end{Bmatrix} = \begin{Bmatrix} F_{\mathrm{m}} \\ F_{\mathrm{e}} \end{Bmatrix} \tag{5}$$

where M_{mm} is the mass matrix, C_{mm} is the damping matrix, K_{mm} is the mechanical stiffness matrix, K_{me} is the piezoelectric matrix, K_{ee} is the dielectric matrix, q_{m} is the mechanical degrees of freedom vector, q_{e} is the electric degree of freedom vector, F_{m} is the mechanical load vector and F_{e} is the electric charge vector. The expressions for those matrices and vectors are detailed below,

$$M_{\mathrm{mm}} = \int_{\Omega} \rho [N_{\mathrm{m}}]^{\mathrm{T}} [N_{\mathrm{m}}] \, \mathrm{d}V \tag{6}$$

$$K_{\mathrm{mm}} = \int_{\Omega} [B_{\mathrm{m}}]^{\mathrm{T}} [C] [B_{\mathrm{m}}] \, \mathrm{d}V \tag{7}$$

$$K_{\mathrm{me}} = -\int_{\Omega} [B_{\mathrm{m}}]^{\mathrm{T}} [e] [B_{\mathrm{e}}] \, \mathrm{d}V \tag{8}$$

$$K_{\mathrm{ee}} = \int_{\Omega} [B_{\mathrm{e}}]^{\mathrm{T}} [\chi] [B_{\mathrm{e}}] \, \mathrm{d}V \tag{9}$$

$$F_{\mathrm{m}} = \int_{S} F^{\mathrm{T}} N_{\mathrm{m}} \, \mathrm{d}S + \int_{\Omega} \rho b^{\mathrm{T}} N_{\mathrm{m}} \, \mathrm{d}V \tag{10}$$

$$F_{\mathrm{e}} = -\int_{S} Q N_{\mathrm{e}} \, \mathrm{d}S - \int_{\Omega} q N_{\mathrm{e}} \, \mathrm{d}V \tag{11}$$

where N_{m} and N_{e} are the mechanical and electrical shape functions, and B_{m} and B_{e} are the mechanical and electrical differential operators. In this work, a Rayleigh damping matrix is used. It is obtained as a linear combination of the mass and stiffness matrices.

A layerwise algorithm is used for the through-thickness integration. For this purpose a change in integration limits and weights is performed and the original integral is expressed as a sum of integrals over each layer,

$$\int_{-1}^{1} f(t) \, \mathrm{d}t = \sum_{k=1}^{n} \left(\int_{t^{k-1}}^{t^k} f^k(t) \, \mathrm{d}t \right). \tag{12}$$

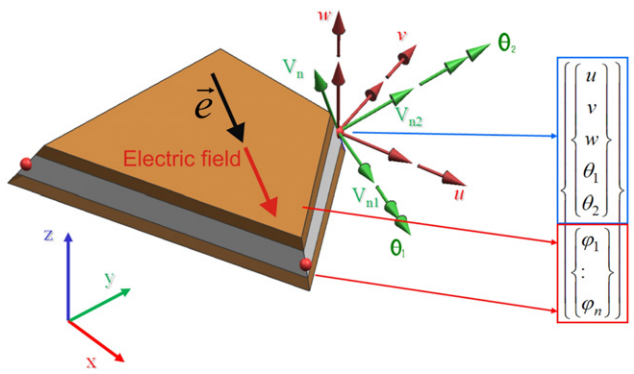

Figure 2. Piezoelectric finite element shell.

The total number of layers is denoted by n. If t^{s} and w^{s} are sampling points and weights for the interval -1 to $+1$, respectively, the sampling points and weights for the interval t^{k-1} to t^k are calculated according to the following equations (Bathe 1996),

$$\tilde{t}^{\mathrm{s}} = \frac{t^{k-1}+t^k}{2} + \frac{t^k - t^{k-1}}{2} \times t^{\mathrm{s}} \tag{13}$$

$$\tilde{w}^{\mathrm{s}} = \frac{t^k - t^{k-1}}{2} w^{\mathrm{s}} \tag{14}$$

where

$$t^k = t^{k-1} + 2 \times \text{layer thickness/total thickness}. \tag{15}$$

Using this integration method, the piezoelectric coupling matrix can be obtained as follows,

$$[K_{\mathrm{me}}] = \sum_{k=1}^{n} \int_{t^{k-1}}^{t^k} \int_{-1}^{+1} \int_{-1}^{+1} [B_{\mathrm{m}}]^{\mathrm{T}} [e] [B_{\mathrm{e}}] |J| \, \mathrm{d}r \, \mathrm{d}s \, \mathrm{d}t \tag{16}$$

where $|J|$ is the Jacobian matrix determinant. The same procedure can be applied for the other matrix and vector integrals.

2.1. Element mechanical behaviour

A single layer approach is used for mechanical variables. The mechanical behaviour of the element is deduced in accordance with the Reissner–Mindlin hypothesis and is based on the solid degenerated approach originally proposed by Ahmad, Irons and Zienkiewicz (A–I–Z) (Ahmad *et al* 1970). The shear locking effect is minimized through the use of mixed interpolation of tensorial components (MITC) (Bathe and Dvorkin 1986, Kögl and Bucalem 2005a, 2005b). As described in Bathe (1996), the element geometry interpolation is obtained by considering the nodal spatial coordinates, the nodal tern ($V_{\mathrm{n1}}, V_{\mathrm{n2}}, V_{\mathrm{n}}$) and nodal thickness. The element has five degrees of freedom per node, three spatial displacement u, v and w and two rotations θ_1 and θ_2. The nodal degrees of freedom define the kinematics of any point inside the element. Figure 2 shows a generic element with the nodal variables.

2.2. Element electromechanical behaviour

As outlined before, the electric field in PFCPIE devices is not uniform along the piezoelectric fibres. However, a simpler model can be employed in order to carry on a macro-electromechanical analysis. The proposed element takes advantage of two main issues, namely the homogenization of the material properties and the assumption that a uniform and constant (not in time but in space) electric field arises inside the device when electrodes are polarized (Bent and Hagood 1997). The combination of both assumptions gives the element the ability to represent the macro-electromechanical behaviour of the PFCPIE device. The piezoelectric shell finite element proposed supports the inclusion of several layers of different materials and orientations in the case of non-isotropic media. In particular, every piezoelectric layer admits a particular material orientation, which also defines the electric field direction based on the direction of maximum longitudinal piezoelectric coupling. This direction is defined by vector $\vec{e}$ and coincides with the fibre direction.

In general terms, the electric field can be expressed as,

$$E_i = -\frac{\partial \varphi}{\partial x_i}. \tag{17}$$

Each piezoelectric layer introduces one electric node with the corresponding electric potential applied to one electrode terminal as one degree of freedom, the other terminal is assumed to be grounded.

Inside each piezoelectric layer, equation (17) can be stated as follows,

$$\vec{E} = -\frac{\varphi}{p}\vec{e} \tag{18}$$

where $\vec{e}$ is a unit vector denoting the fibre direction, and p is the electrode spacing.

In the finite element context, the electric field inside each piezoelectric layer could be expressed in terms of the electric potential applied to the corresponding electrode as,

$$\begin{Bmatrix} E_x \\ E_y \\ E_z \end{Bmatrix}_{\text{layer } j} = -\frac{1}{p_{\text{layer } i}} \begin{bmatrix} e_x \\ e_y \\ e_z \end{bmatrix}_{\text{layer } j} \{\varphi\}_{\text{layer } j} \tag{19}$$

where $p_{\text{layer } j}$ and $\vec{e}_{layer\ j}$ are the electrode finger distance and the unitary fibre director vector, respectively for layer j. Equation (19) can also be written as,

$$\begin{Bmatrix} E_x \\ E_y \\ E_z \end{Bmatrix}_{\text{layer } j} = -\left[f_1 \frac{1}{p_1} \begin{bmatrix} e_x \\ e_y \\ e_z \end{bmatrix}_1 \cdots f_k \frac{1}{p_k} \begin{bmatrix} e_x \\ e_y \\ e_z \end{bmatrix}_k \cdots f_n \frac{1}{p_n} \begin{bmatrix} e_x \\ e_y \\ e_z \end{bmatrix}_n \right] \begin{Bmatrix} \varphi_1 \\ \vdots \\ \varphi_n \end{Bmatrix} \tag{20}$$

where,

$$f_k = \begin{cases} 1 & \text{if } j = k \\ 0. & \end{cases} \tag{21}$$

Matrix $[B_{\mathrm{e}}]$ results,

$$[B_{\mathrm{e}}] = -\left[f_1 \frac{1}{p_1} \begin{bmatrix} e_x \\ e_y \\ e_z \end{bmatrix}_1 \cdots f_k \frac{1}{p_k} \begin{bmatrix} e_x \\ e_y \\ e_z \end{bmatrix}_k \cdots f_n \frac{1}{p_n} \begin{bmatrix} e_x \\ e_y \\ e_z \end{bmatrix}_n \right]. \tag{22}$$

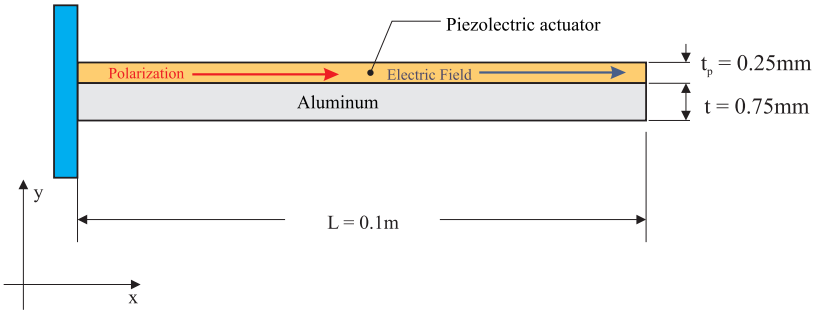

Figure 3. Actual geometry of the piezoactuated beam.

3. Element test

In order to assess the static element behaviour, a cantilever beam with bonded piezoelectric actuators is first analysed. See figure 3. The numerical model is carried out by employing the multilaminar piezoelectric shell formulation presented in this paper.

In order to compare the results, a detailed model with bidimensional plane stress solids is also performed with ABAQUS (2006). Results for a successive mesh refinement are compared. Finally, finite element results are also compared with the analytical solution obtained for the piezoactuated beam using the Euler–Bernoulli beam theory (Agrawal and Treanor 1999).

The material properties used for the beam and piezoelectrics actuators are presented in table 1. The actuator is polarized with interdigitated electrodes. The homogenized electric field inside the piezoelectric actuator depends on the electric potential applied and on the electrode spacing. In this example, an electric potential of 1000 V was applied to induce an electric field of 1.0×10^6 V m^{-1} for an electrode spacing of 1.0×10^{-3} m.

The beam was first modelled with the present shell formulation. Each shell element was considered to have four layers: three equal layers for the aluminium zone and one layer for the actuator. A successive mesh refinement was performed ranging from one single element up to 500 for the length of the beam. Only one element in the beam width was used. The solution of this particular problem is independent of the beam width. Therefore, in order to avoid numerical difficulties due to high aspect ratios, the elements width was lowered in correspondence to the longitudinal mesh refinement. An electric potential of 1000 V was imposed on the piezoelectric layer of each shell element.

The piezoactuated beam was also analysed with the commercial program ABAQUS (2006). The active layer was modelled with ABAQUS/CPS4E bilinear solid plane stress piezoelectric elements, while ABAQUS/CPS4 full integration and ABAQUS/CPS4R reduced integration elements were used for the passive zone. Eight elements were used across the height of the beam, and the number of elements along the beam varied from 5 to 500. The two upper element layers correspond to the actuators. A uniform electric field was introduced by imposing a gradually increasing nodal electric potential in the direction of the x coordinate axis. The increment in nodal electric potential is calculated with the simple expression

$$\Delta\varphi = \text{desired electric field} \times \text{spanwise mesh spacing}. \quad (23)$$

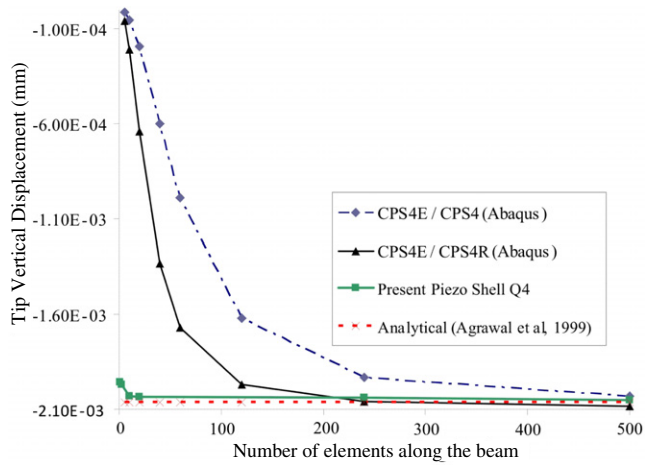

Figure 4. Tip displacement induced by an electric field of 1.0×10^6 V m^{-1}. Convergence plots for successive mesh refinement.

The tip displacement induced by the piezoelectric actuator was computed for different mesh refinement levels and different types of elements (present piezo shell Q4, ABAQUS CPS4E/CPS4 and ABAQUS CPS4E/CPS4R).

Results obtained with the present formulation and ABAQUS model are presented in figure 4 and compared with analytical results of the Bernoulli beam theory model from Agrawal and Treanor (1999).

It can be observed that, even using reduced integration techniques in order to avoid element locking, solid plane elements give results with an acceptable error only for relative high mesh refinement levels and the correspondingly elevated number of degrees of freedom. In contrast, very accurate results are obtained with the present shell formulation using only a few elements along the span. For 20 elements the relative error is about 1.4%. Using the present formulation, both the electric and mechanical degrees of freedom are notably reduced.

To some extent, the numerical experiments performed with solid elements in ABAQUS can be considered as a full layerwise theory. Regarding this aspect, figure 4 shows that

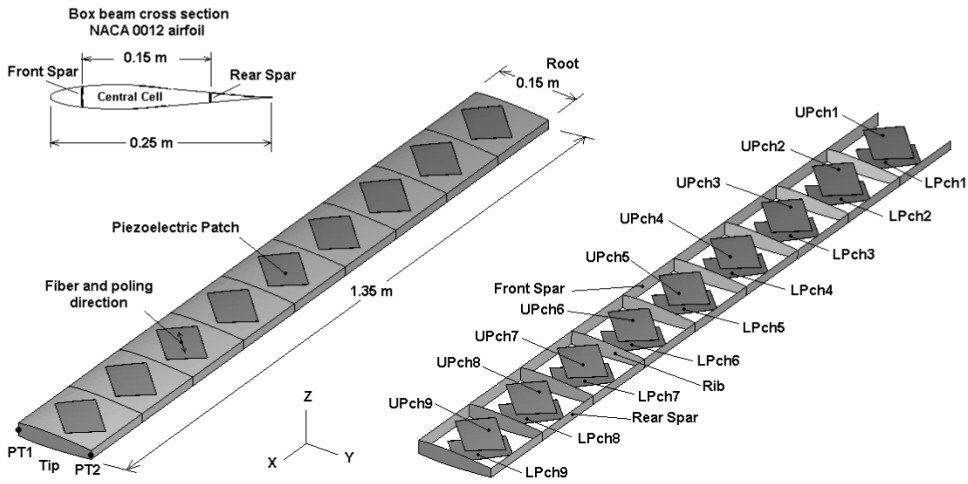

Figure 5. Geometry of the closed box beam analysed by Guennam and Luccioni (2006).

similar results can be obtained with the present FE formulation (Piezo Shell Q4) that combines a single layer approach for the mechanical degrees of freedom with a multilayer approach for the electric field. These results are very encouraging because the total number of degrees of freedom (DOF) is strongly reduced when the proposed finite element is used.

4. Actuated single cell composite beam

The objective of this section is to use the proposed shell FE in the design of aero-spatial structures and the assessment of structural vibration control systems in this kind of application. Closed composite beams are widely used in aircraft wings and helicopters blades.

First, the presented formulation is employed to model the closed box beam already analysed by the authors in a previous paper using ABAQUS (Guennam and Luccioni 2006), and the results of both finite element models are compared. The model corresponding to a thin walled single cell box beam with piezoelectric fibre composite patches bonded to its skin is analysed. Patch fibres are oriented at ±45° with respect to the beam longitudinal axis. The geometry and the piezoelectric patch layout are shown in figure 5.

The first analysis corresponds to a static tip twist induced by a 500 V electric potential applied to each piezoelectric actuator. A tip twist angle of 0.067° is obtained by Guennam and Luccioni (2006) and 0.069° with the present formulation, thus representing a difference of 2.5% with 30% less DOFs.

The control system was designed based on the present formulation and compared with the control system based on the previous model (Guennam and Luccioni 2006). For the addressed problem, 30% less DOFs were employed by using the present formulation. A comparison of the transient response produced by a concentrated 20 N force applied to point PT1 (tip of the front spar), with a temporal variation of a 0.1 s. step is performed. Figure 6 shows the comparison of closed-loop transient response obtained with both models.

Figure 7 shows the temporal variation of the control voltage applied to actuator number 1, on the top and nearest to the beam root.

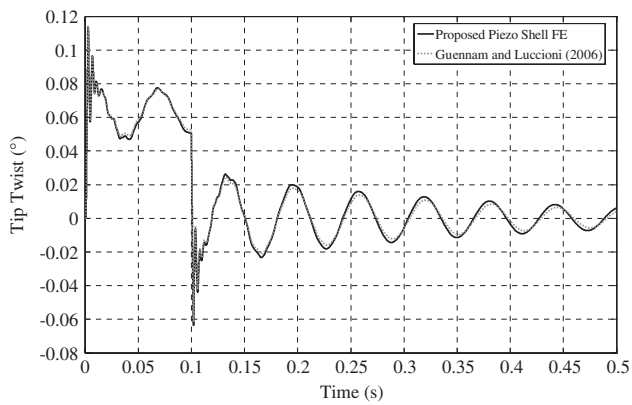

Figure 6. Tip twist transient closed-loop response—comparison with Guennam and Luccioni (2006).

The results are almost coincident. The small differences observed could be attributed to the numerical process employed to condense the stiffness and mass matrices obtained with ABAQUS before exporting them to MATLAB, where the control system is designed and assessed.

In a second stage the finite element presented is employed to model a twist actuated helicopter blade experimentally tested by DuPlessis and Hagood (1996). They used an AFC actuator with the electromechanical properties presented in table 1. First, the actuated box beam is numerically analysed with the proposed FE and numerical and experimental results for static linear response are compared. Later, a control system for the actuated box beam is designed and a dynamic analysis is performed.

Figure 8(a) shows a general layout of the closed box single cell composite beam with piezoelectric patches oriented ±45° with respect to the spanwise (z) direction. Figure 8(b) shows the active and passive laminates and thickness.

The passive structure is made of a glass/epoxy composite that is supposed to have a linear elastic behaviour with the mechanical properties specified in table 1. The laminate is made up of two layers oriented at 0° with respect to the spanwise direction. The active area consists of six piezoelectric

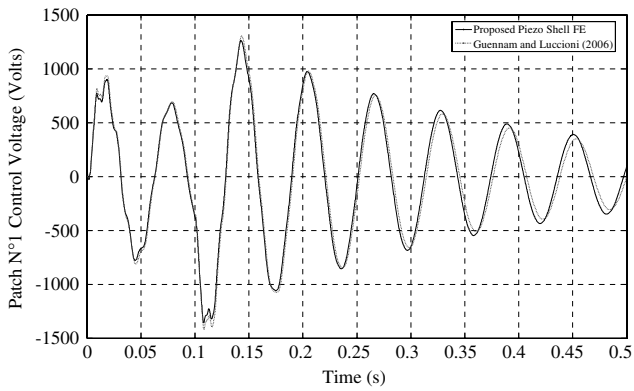

Figure 7. Control voltage applied to patches UPch1 (nearest to root)—comparison with Guennam and Luccioni (2006).

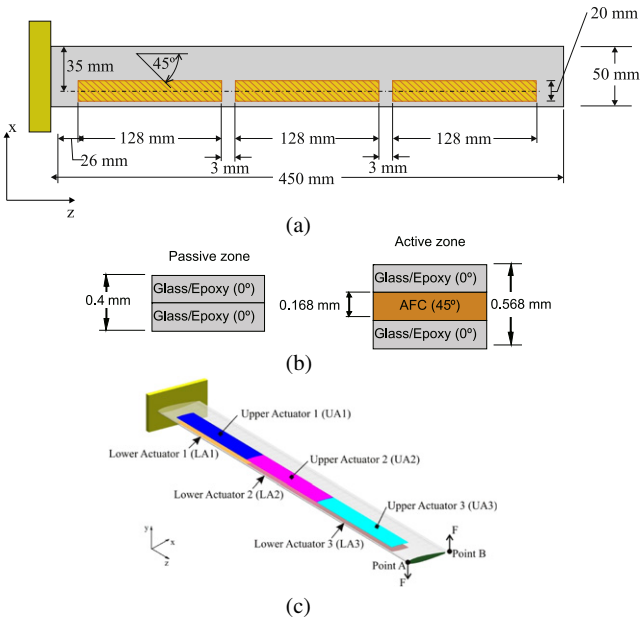

Figure 8. General layout of the closed box beam analysed, measures in mm. (a) Plant view with main dimensions. (b) Active and passive zone laminated thickness. (c) Spatial structure.

fibre composite actuator patches embedded between the two layers of epoxy/glass composite and oriented at ±45°. This aspect is depicted in figure 8(b). Each actuator is considered to be controlled independently.

The whole structure is modelled using the shell element formulated. The finite element mesh is shown in figure 9. Fifty elements along the span and twelve along the chord with smaller elements near the leading edge were used. The mesh has 1224 nodes and 1209 elements. The elements at the tip represent a rib.

A set of constraints was imposed between the electric DOFs of the piezoelectric layers corresponding to each one of the six actuators. In this way, only 6 electric degrees of freedom (one for each actuator) are active in the model.

For the present analysis a very low structural damping, 1% for all modes, and a Rayleigh proportional damping are considered.

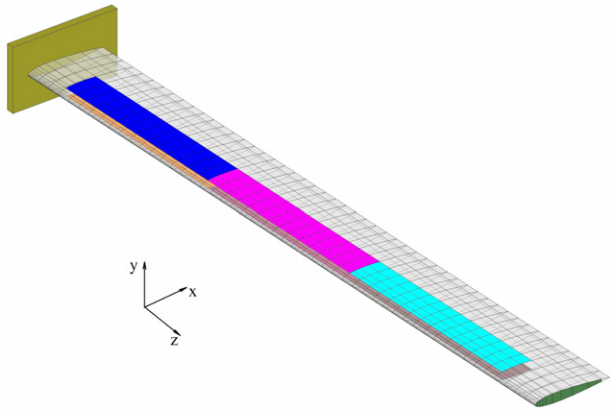

Figure 9. Finite element model of the actuated closed box beam.

4.1. Static analysis

For the closed box beam experimentally analysed by DuPlessis and Hagood (1996), the twist induced by the AFC piezoelectric actuators is first determined for a constant voltage supplied to the actuators terminals. The tip twist angle α was computed from tip node displacements. The tip twist α achieved for 500 V (equivalent uniform electric field $E_{\mathrm{eq}} = \frac{500}{p_{\mathrm{AFC}}}$) of actuation signal is 0.36°. This result represents a difference in 4.5% with respect to the 0.35° experimentally obtained by DuPlessis and Hagood (1996) with 500 V applied to electrodes in the experiment. This could be due to non-modelled features and model parameter discrepancies.

Park and Kim (2005) modelled the same problem using piezoelectric actuators of active fibre composite (AFC) and macro-fibre composite (MFC) types. The actuated box beam provided with MFC actuators was also modelled with the present piezo shell finite element and the results obtained were compared. The corresponding tip twist calculated for 500 V (equivalent uniform electric field $E_{\mathrm{eq}} = \frac{500}{p_{\mathrm{MFC}}}$) of actuator voltage is 0.94°, which differs by 6% from the result reported by Park and Kim (2005).

Even though the same voltage is applied in AFC and MFC, the difference in electrode spacing in both devices gives a different electric field inside the actuators. This explains the increment in tip twist angle induced by MFC actuation. In the numerical experiments performed in this work, the uniform electric field considered for the MFC actuator is $E_{\mathrm{eq}}^{\mathrm{MFC}} = 943\ \mathrm{kV\ m^{-1}}$, while for the AFC is $E_{\mathrm{eq}}^{\mathrm{AFC}} = 416\ \mathrm{kV\ m^{-1}}$.

4.2. Control analysis

The proposed finite element is employed in this section to obtain the equations of motion used as starting point of the control analysis of the NACA0012 closed box. For this purpose, the finite element model is recast in the state space form (Mitra *et al* 2004) and the LQR technique is employed for the controller design (Narayanan and Balamurugan 2003). The frequency response of the controlled system is evaluated and, finally, a transient simulation is performed. A similar analysis was performed by Guennam and Luccioni (2006). However, the numerical model was based on shell elements for

the passive structure and piezoelectric solid elements for the actuators. Using the present piezoelectric shell formulation, the computational cost is lower and the imposition of electric boundary conditions is simpler.

4.3. State space modelling

From equation (5), and following a simple process consisting of matrix and vector partitioning, restrained DOFs are separated from the free ones. The modified equation obtained enables the introduction of perturbations and the imposition of control voltages in a relatively easy way. This modified FE equation system is then recast in a state space form to provide a standard mathematical basis for control design and performance assessment.

The state space model is expressed by means of equation (24), where $\{x(t)\}$ is the state vector, $[A]$ is the system matrix, $[B]$ is the control matrix, $\{u(t)\}$ is the control input (electric potentials), $[E]$ is the perturbation matrix and $\{f^{\text{pert}}(t)\}$ is the perturbation vector, which includes mechanical forces, electric charges and displacements, velocities and accelerations prescribed on certain points of the structure.

$$\{\dot{x}(t)\} = [A]\{x(t)\} + [B]\{u(t)\} + [E]\{f^{\text{pert}}(t)\}. \tag{24}$$

Control matrix $[B]$ is established, taking into account that control actions are provided only by piezoelectric actuators. These actuators are driven by voltages applied on those nodes whose electric DOFs are labelled as restrained.

Electrical perturbations are ignored. The perturbation matrix $[E]$ is derived assuming only mechanical perturbations, namely displacements, velocities, accelerations, forces and moments acting on certain portions of the structure.

As mentioned before, state feedback is used, so that the control signal $u(t)$ is given by

$$\{u(t)\} = -[G]\{x(t)\} \tag{25}$$

where $[G]$ is the gain matrix that must be determined.

4.4. Controller design

The gain matrix is calculated in such a way that the feedback law given by equation (25) minimizes the quadratic performance index,

$$J = \int_0^\infty (\{x\}'[Q]\{x\} + \{u\}'[R]\{u\})\,\mathrm{d}t. \tag{26}$$

The matrices $[Q]$ and $[R]$ in equation (26) are positive semidefinite and positive definite weighting matrices, respectively. These matrices provide a desired balance between the state variable response and control efforts. The following weighting matrices are used in this paper,

$$[Q] = \gamma_q[I] \qquad [R] = \gamma_r[I] \tag{27}$$

γ_q and γ_r are real numbers varying from 0 to ∞.

The system output equation is,

$$\{y(t)\} = [C]\{x(t)\} \tag{28}$$

where $\{y(t)\}$ is the output vector and $[C]$ is the output matrix.

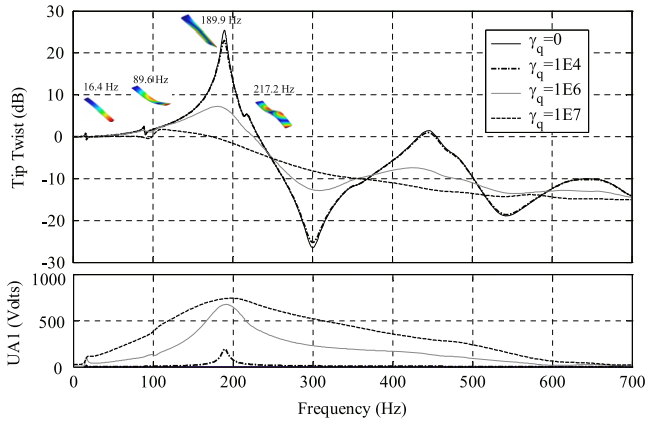

Figure 10. Frequency response—tip twist angle and control voltage applied to upper actuator No. 1 (UA1).

Once the gain matrix is determined, equation (24) adopts the following form,

$$\{\dot{x}(t)\} = [A_c]\{x(t)\} + [E]\{f^{\text{pert}}(t)\} \tag{29}$$

where $[A_c]$ is the closed-loop system matrix which is given by,

$$[A_c] = [A] - [B][G]. \tag{30}$$

From closed-loop state space equation, the effects that the control system has on the structure can be analysed (Narayanan and Balamurugan 2003, Guennam and Luccioni 2006).

4.5. Frequency response

In order to evaluate the steady state dynamic response of the structure being considered, a frequency response analysis is performed. The excitation is a generic harmonic twisting moment applied to the tip, $M = M_0 \mathrm{e}^{-\mathrm{i}\omega t}$, $M_0 = 0.125$ (N m).

The frequency response corresponding to four gain parameter γ_q values between, 0 and 10^7, are presented in figure 10. The effect of the controller is clearly manifested. Up to 25 dB attenuation in a resonance condition of the first torsional mode is introduced by the controller. This represents an attenuation level of 0.01 dB V^{-1}. Because of the linear behaviour assumption, this value could be seen as a system characteristic. Imposing 800 V as a maximum operational voltage for the actuators, an attenuation capability of 15 dB could be expected for the first torsional mode. The modal shapes for the first four modes are presented in figure 10 in correspondence with the modal peak amplitudes.

4.6. Transient response

For a transient response analysis, the box beam is considered to be excited with a couple, of value $M = 0.25$ (N m), applied to the tip and modulated in time by a step function of 0.05 s duration represented in figure 11.

The temporal response for the different values of the parameters used to determine the gain matrix is compared in figure 12.

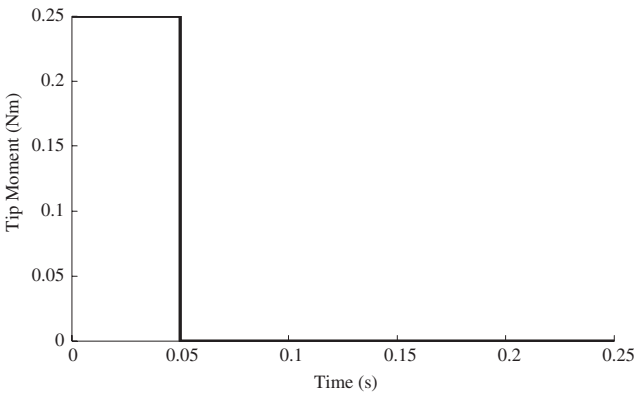

Figure 11. Tip perturbation twisting moment.

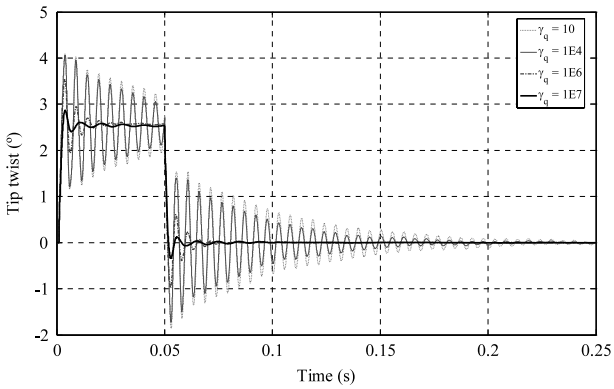

Figure 12. Tip twist angle. Transient response for different gain values.

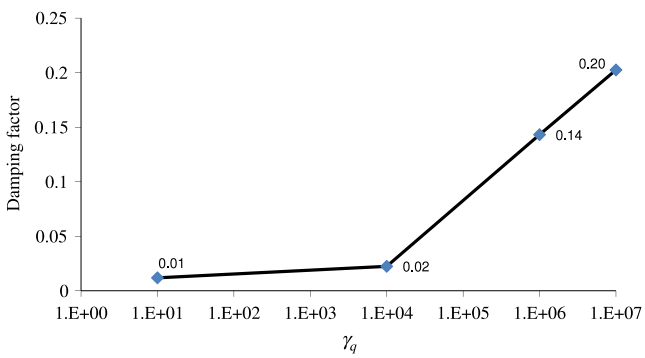

Figure 13. Damping factor introduced by the control system.

The low structural damping is manifested in figure 12 by the open-loop response. For the closed-loop response, an increasing damping is introduced by the controller. For $\gamma_q = 1 \times 10^6$, the vibration attenuates almost completely in 0.025 s. For $\gamma_q = 1 \times 10^7$ this time is 0.015 s and the damping factor introduced by the controller is 0.2, approximately as shown in figure 13, where damping factor in the function of γ_q for the first torsional mode is drawn.

Figures 14 and 15 show the control voltages for the actuators close to the root and the tip of the box beam. As expected, the maximum voltages are applied to the root actuators because a state feedback controller is employed. Similar results could be found in the previous work of

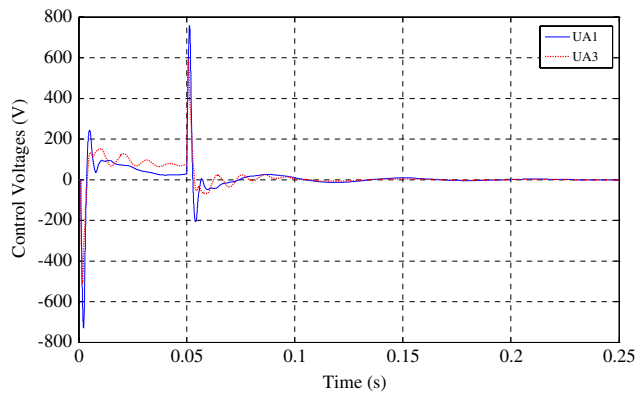

Figure 14. Control voltage on upper actuators No. 1 (UA1) and No. 3 (UA3) for gain parameter $\gamma_q = 1.0 \times 10^7$.

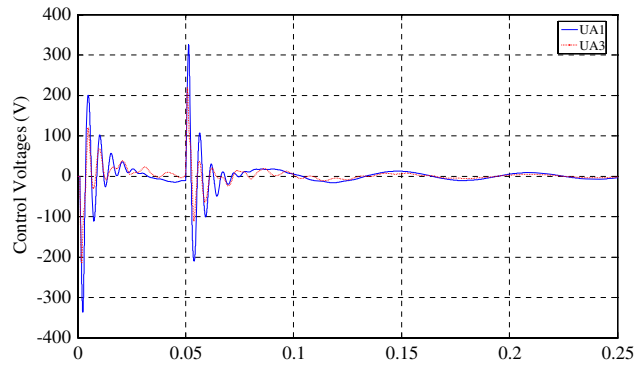

Figure 15. Control voltage on upper actuators No. 1 (UA1) and No. 3 (UA3) for gain parameter $\gamma_q = 1.0 \times 10^6$.

Guennam and Luccioni (2006), where the authors employ solid piezoelectric elements to model the piezoelectric patches. The controller is able to attenuate the torsional vibration without exceeding 800 V of control signals.

5. Concluding remarks

This work introduces a new interpolation scheme for the electric field in piezolaminated composite degenerated shell finite elements. In combination with an existing finite element shell formulation, the present electric field interpolation allows the modelling of piezoelectric composite laminates, polarized with interdigitated electrodes, in a simple and natural way.

In order to validate the present formulation a cantilever piezoactuated beam was modelled and numerical results were compared with an analytic solution of the corresponding Bernoulli model. A 1% difference in tip deflection induced by piezoelectric actuator was obtained.

A numerical modelling of a piezoelectric actuated closed box beam was performed. At the first stage static numerical analysis was performed in order to compare numerical results with experimental results obtained by other authors. Numerical and experimental results are in good agreement, with a maximum difference of 6% in the actuator induced static twist.

The frequency response analysis shows that attenuations up to 25 dB (0.01 dB V^{-1}) could be obtained in the torsional

modes of the actuated closed box analysed. The transient response against tip twisting moment was evaluated for different values of gain. In this way, a damping factor of 0.2 was introduced in the first torsional model with 800 V maximum control voltages. In the example addressed in this work the voltage levels do not exceed 800 V, levels for which piezoelectric nonlinear effects are expected to be negligible.

Full linear (geometrical and material) behaviour was assumed, hence extrapolations for different load magnitudes could be made but verifications of these linear assumptions are needed for each particular case.

With the present formulation numerical models of active structures can be performed, retaining the important aspects of the physical model being analysed, but with a moderate number of DOFs and allowing a relatively easy way of imposing the electrical boundary conditions. Two modelling approaches for the same problem were compared. One approach uses piezoelectric brick elements and the other is based on the proposed piezoelectric shell finite element. Comparisons between these results reveal that the computational cost is considerably diminished (about 30% less degrees of freedom), while the accuracy of results is retained, when using the proposed shell finite element. Moreover, modelling is notably simplified in the proposed approach, because the electric field is introduced by setting only one degree of freedom per each piezoelectric layer of each element and fewer restraints between electric degrees of freedom are required in order to impose the electric fields in the fibre directions.

Acknowledgments

The financial support of CONICET and the Research Council of National University of Tucumán (CIUNT) is gratefully acknowledged. The authors also wish to thank Amelia Campos for her collaboration in the English revision.

References

ABAQUS 2006 *Standard User's Manual* V6.6 (Providence, RI: Abaqus, Inc.)

Agrawal B N and Treanor K E 1999 Shape control of a beam using piezoelectric actuators *Smart Mater. Struct.* **8** 729–40

Ahmad S, Irons B M and Zienkiewicz O C 1970 Analysis of thick and thin shell structures by curved finite elements *Int. J. Numer. Methods Eng.* **2** 419–51

Allik H and Hughes T J R 1970 Finite element meted for piezoelectric vibration *Int. J. Numer. Methods Eng.* **2** 151–7

Balachandran B, Sampath A and Park J 1996 Active control of interior noise in a three-dimensional enclosure *Smart Mater. Struct.* **5** 89–97

Balamurugan V and Narayan S 2001 Active vibration control of piezolaminated smart beams *Defence Sci. J.* **51** 103–14

Balamurugan V and Narayan S 2008 A piezolaminated composite degenerated shell finite element for active control of structures with distributed piezosensors and actuators *Smart Mater. Struct.* **17** 035031

Bathe K J 1996 *Finite Element Procedures* (Englewood Cliffs, NJ: Prentice-Hall)

Bathe K J and Dvorkin E N 1986 A formulation of general shell elements—the use of mixed interpolation of tensorial components *Int. J. Numer. Methods Eng.* **22** 697–722

Benjeddou A 2000 Advances in piezoelectric finite element modeling of adaptive structural elements: a survey *Comput. Struct.* **76** 347–63

Bent A and Hagood N W 1997 Piezoelectric fibre composites with interdigitated electrodes *J. Intell. Mater. Syst. Struct.* **8** 903–19

Carrera E 1997 An improved Reissner–Mindlin type model for the electromechanical analysis of multilayered plates including piezo-layers *J. Intell. Mater. Syst. Struct.* **8** 232–48

Carrera E 2002 Theories and finite elements for multilayered, anisotropic, composite plates and shells *Archiv. Comput. Methods Eng.* **9** 87–140

Carrera E 2003 A historical review of zig-zag theories for multilayered plates and shells *Appl. Mech. Rev.* **56** 287–308

Chee C, Tong L and Steven G 2000 A mixed model for adaptive plates with piezoelectric for anisotropic actuation *Comput. Struct.* **77** 254–68

Crawley E F and de Luis J 1987 Use of piezoelectric actuators as elements of intelligent structures *AIAA J.* **25** 1373–85

DuPlessis A J and Hagood N W 1996 Modeling and experimental testing of twist actuated single cell composite beams for helicopter rotor blade control *MS Dissertation* Department of Aeronautics and Astronautics, Massachusetts Institute of Technology

Guennam A E and Luccioni B M 2006 FE modeling of a closed box beam with piezoelectric fibre composites patches *Smart Mater. Struct.* **15** 1605–15

Joshi S P 1992 Non-linear constitutive relations for piezoceramic materials *Smart Mater. Struct.* **1** 80–3

Kekana M 2003 A static shape control model for piezo-elastic composite structures *Compos. Struct.* **59** 129–35

Kögl M and Bucalem M L 2005a Analysis of smart laminates using piezoelectric MITC plate and shell elements *Comput. Struct.* **83** 1153–63

Kögl M and Bucalem M L 2005b A family of piezoelectric MITC plate elements *Comput. Struct.* **83** 1277–97

Lammering R 1991 The application of a finite shell element for composites containing piezoelectric polymers in vibration control *Comput. Struct.* **41** 1101–9

Lammering R and Mesecke-Rischmann S 2003 Multi-field variational formulations and related finite elements for piezoelectric shells *Smart Mater. Struct.* **12** 904–13

Lee H J and Saravanos D 2000 A mixed multi-field finite element formulation for termopiezoelectric composite shell *Int. J. Solids Struct.* **37** 4949–67

Lim Y H, Gopinathan S V, Varadan V V and Varadan V K 1999 Finite element simulation of smart structures using an optimal output feedback controller for vibration and noise control *Smart Mater. Struct.* **8** 324–37

Mitra M, Gopalakrishnan S and Bhat M S 2004 Vibration control in a composite box beam with piezoelectric actuators *Smart Mater. Struct.* **13** 676–90

Monkhouse R S C, Wilcox P W, Dalton R P and Cawley P 2000 The rapid monitoring of structures using interdigital Lamb wave transducers *Smart Mater. Struct.* **9** 304–9

Nam C and Kim Y 1995 Optimal design of composite lifting surface for flutter suppression with piezoelectric actuators *AIAA J.* **10** 1897–904

Narayanan S and Balamurugan V 2003 Finite element modeling of piezolaminated smart structures for active vibration control with distributed sensors and actuators *J. Sound Vib.* **262** 529–62

Park J S and Kim J H 2005 Analytical development of single crystal macro fibre composite actuators for active twist rotor blades *Smart Mater. Struct.* **14** 745–53

Reddy J N 1999 On laminated composite plates with integrated sensors and actuators *Eng. Struct.* **21** 568–93

Saravanos D A, Heyliger P R and Hopkins D A 1997 Layerwise mechanics and finite element for the dynamic analysis of piezoelectric composite plates *Int. J. Solids Struct.* **34** 359–78

Suleman A and Costa A P 2004 Adaptive control of an aeroelastic flight vehicle using piezoelectric actuators *Comput. Struct.* **82** 1303–14

Suleman A and Venkayya V B 1995 A simple finite element formulation for a laminated composite plate with piezo-electric layers *J. Intell. Mater. Syst. Struct.* **6** 776–82

Sungsoo N and Librescu L 1998 Oscillation control of cantilevers via smart material technology and optimal feedback control: actuator location and power consumption issues *Smart Mater. Struct.* **7** 833–42

Thirupathi S R, Seshu P and Naganathan N G 1997 A finite static analysis of smart turbine blades *Smart Mater. Struct.* **6** 607–15

Varadan V V, Chin L and Varadan V K 1993 Finite element modeling of flextensional electroacoustic transducers *Smart Mater. Struct.* **2** 201–7

Wang Q and Quek S T 2002 Enhancing flutter and buckling capacity of a column by piezoelectric layers *Int. J. Solids Struct.* **39** 4167–80

Wang Z, Chen S and Han W 1999 Integrated structural and control optimization of intelligent structures *Eng. Struct.* **21** 183–91